Progress In Electromagnetics Research Letters, Vol. 67, 1–6, 2017

Validation of a Convolution Integral for Conductivity Imaging

Joe R. Feldkamp[1, *] and Stephen Quirk[2]

Abstract—Magnetic induction tomography has been under consideration for imaging electrical conductivity distributions within the human body. Multi-coil systems are most commonly employed for this task, requiring a numerical solution of Maxwell's equations at each position of the coil array. An alternative uses a single coil placed near the conductive target while measuring coil self-impedance changes at a number of unique locations. Recently, a closed-form solution of Maxwell's equations, in the form of a 3D convolution integral, was found for a single coil consisting of concentric circular loops that relates impedance change (loss) to an arbitrary conductivity. Its development required spatially uniform permittivity and permeability, yet showed quantitative agreement with experiment. Here, we provide a much more rigorous test of the convolution integral in experiments that allow large permittivity changes across coil dimensions. Loss is measured while the coil is placed at known positions relative to plastic columns of variable diameter which are filled with salt solutions of varying conductivity. In all cases, coil loss varies linearly with conductivity and with zero intercept. Quantitative agreement is observed only when column diameter is greater than or equal to coil diameter. Because of linearity, the convolution integral is useful for image reconstruction, though contrast could be either reduced or enhanced in those circumstances when relative permittivity change exceeds ~ 70.

1. INTRODUCTION

Efforts to image electrical conductivity within the human body have primarily relied upon two differing imaging modalities — either electrical impedance tomography (EIT) [1, 2] or magnetic induction tomography (MIT) [3, 4]. EIT requires electrode contact with the object under test in order to inject electrical currents, while additional attached electrodes serve as sensors to help determine current distribution throughout a portion of the body. MIT instead relies upon the ability of an induction coil to induce eddy currents via an EM excitation field, making contact unnecessary. These eddy currents create their own secondary field which can be detected in a second independent coil *or* in the primary excitation coil itself [5, 6]. As stated by Zaman et al. [6], the former requires an analysis of transfer impedance for a primary and secondary coil placed near a test object while the latter involves a calculation of self-impedance of the primary coil when placed in the immediate vicinity of the target. A multi-coil system has the distinct disadvantage of requiring a numerical solution of Maxwell's equations for each position of the coil array relative to target, which is needed for the "forward problem" prior to image reconstruction.

A single mobile coil is not only physically simpler to manage, but progress has been made at finding closed form solutions [5–8] that could alleviate the need for a much more laborious effort toward solving the forward problem. These analytical approaches, though formidable in form, offer an ability to see a clear connection between measured impedance change, δZ, and basic problem parameters — such as conductivity and target geometry. Nevertheless, these closed-form expressions all have the difficulty that conductivity is treated as spatially invariant within the target geometries studied, making them

Received 14 January 2017, Accepted 8 March 2017, Scheduled 16 March 2017
* Corresponding author: Joe R. Feldkamp (jrfeldcinci@gmail.com).
[1] Kimberly-Clark Corp., Neenah, WI, USA. [2] Kimberly-Clark Corp., Roswell, GA, USA.

unsuitable candidates for conductivity imaging. More recently [9], a closed-form expression relating impedance change, which we will call inductive loss since impedance change shows up as a dissipative resistive load in series with the coil, was developed that imposes no requirement on the electrical conductivity distribution. Though this makes it an attractive candidate for conductivity imaging, the expression was derived at the expense of treating permittivity and permeability as spatially uniform. In this short communication, we examine the consequences of the uniform permittivity approximation. We provide experimental results that justify the use of the convolution integral, which has no adjustable parameters requiring calibration, for conductivity imaging. If permittivity imaging was desired, other modalities such as electrical capacitance tomography [10] have been proposed.

2. CONVOLUTION INTEGRAL FOR IMPEDANCE CHANGE

The recently developed closed-form analytical expression [9] for inductive loss (or impedance change) may be written as a 3D convolution integral that convolves conductivity $\sigma(\vec{r})$ with the kernel $G(\vec{r}_c)$. Given the rotation matrix $\tilde{R}$, vector $\vec{r}_c = \tilde{R}^T(\vec{r} - \vec{c})$ locates the field point in the coordinate system of the coil, and vector $\vec{c}$ locates the coil center relative to the lab frame origin:

$$\delta Z(\vec{c}) = \int \sigma(\vec{r}) G\left(\tilde{R}^T(\vec{r} - \vec{c})\right) dxdydz \tag{1}$$

The coil coordinate system consists of an orthogonal set of Cartesian axes located at the coil center with Z axis normal to the coil plane, while the kernel is given in terms of a summation over the concentric circular loops that comprise the coil:

$$G(\vec{r}_c) = \frac{\mu^2\omega^2}{4\rho\pi^2} \sum_{j,k} \sqrt{\rho_j \rho_k} Q_{1/2}(\eta_j) Q_{1/2}(\eta_k) \tag{2}$$

Arguments for the circularly symmetric toroid (or ring) function $Q_{1/2}$ lie in the interval $1 < \eta < \infty$ and are related to field position by:

$$\eta_j = \frac{\rho^2 + \rho_j^2 + z_c^2}{2\rho\rho_j}; \quad \eta_k = \frac{\rho^2 + \rho_k^2 + z_c^2}{2\rho\rho_k} \tag{3}$$

Using any suitable fixed laboratory coordinate system, other symbols are defined by:

$\sigma(\vec{r})$: *Electrical conductivity (real part) at field position (lab)*: $\vec{r} = x, y, z$

ρ_k: *Cylindrical radial distance from coil axis to wire loop 'k'*

ρ: *Cylindrical radial distance from coil axis to field point*

z_c: *Perpendicular distance from coil plane to field point*

μ: *Magnetic permeability — considered uniform*

ω: *Angular frequency.*

The function $G(\vec{r}_c)$ is rapidly evaluated through use of a hypergeometric series for the toroidal functions [12]. If the coil is not rotated relative to the lab frame, then the rotation matrix is just the identity matrix. Inductive loss is computed at 12.5 MHz by using a finite element discretization of the convolution integral. This is accomplished by expanding the electrical conductivity into the usual superposition of shape functions. Here, we use a linear basis set on deformed prismatic elements [[13], Fig. 3], with 9-point integration over each element.

3. INDUCTIVE LOSS MEASUREMENT

Coil geometry and construction is identical to that described previously [9] — two planes of concentric circular loops, spaced 0.5 mm, prepared on a double-layer printed circuit board (PCB). Loop traces are 0.5 mm wide, built from 2 oz. copper, having radii of 4, 8, 12, 16 and 20 mm, all wired in series, giving ten loops total. There is a 1 mm buildup of PCB material on the side of the coil facing outward, so that there is at least a 1 mm separation between coil and target. Coil inductance, L, is calculated from

Equations (5) and (6) of earlier work [9] — the latter repeated here in more general form in terms of loop self-inductance, L_{sj}, and mutual inductances between loops, M_{jk}:

$$L = N_{\text{layers}}^2 \left(\sum_{j=1}^{5} L_{sj} + \sum_{j,k=1}^{5} M_{jk} \right); \quad j \neq k \tag{4}$$

In our case, there are two layers, so that a factor of four multiplies each sum. Equation (4) is a reasonable approximation for our coil's inductance provided that the distance between layers is very small compared with loop radii. Inductance for our coil was calculated to be 2.155 μH, which is used in all computations here and agrees with measurement to within 1% [9].

Coil loss, known to be weak and difficult to measure [11], is computed from a change in the real part of admittance, δY_{re}, relative to the free space value, which subtracts the effect of any loss intrinsic to the coil. Given inductance L and frequency ω, coil loss is computed from the formula:

$$\delta Z = \omega^2 L^2 \delta Y_{re} \tag{5}$$

Thus, two admittance measurements are needed — one in free space that avoids interaction with nearby conductive objects, and then subsequent measurements in the immediate vicinity of a conductive specimen. When making 20 to 30 free space measurements at 12.5 MHz, admittance standard deviation is typically ~ 0.11 μS. Additional details are found in [9].

4. COLUMN EXPERIMENTS

In our previous paper, measured coil loss was shown to give quantitative agreement with theory when the coil was placed at varying distances above and parallel to a large tank of aqueous potassium chloride — the tank had a diameter $\sim 6\times$ larger than the coil diameter. The reason for using such a large tank is associated with the known "reach" of the coil in the coil plane [14]. The tank was sufficiently large that an appreciable EM field would not likely have intercepted the salt solution at its lateral boundaries, so that the impact of a sudden change in relative permittivity would be minor.

But here, we are concerned with smaller systems that would permit appreciable EM field interception of target boundaries, and considering these will help us better understand the uniform permittivity approximation. This is accomplished by placing the coil in contact with the wall of a small-diameter column that contains a salt solution, such that the plane of the coil is parallel to the column axis and the coil axis intersects the column axis — see Figure 3 for sketch. We tested five different column internal diameters — 1.75 cm (wall thickness = 3.0 mm), 2.3 cm (wall thickness = 3.6 mm), 3.98 cm (wall thickness = 4.2 mm), 5.1 cm (wall thickness = 4.6 mm) and 7.7 cm (wall thickness = 6.0 mm). Column material is PVC (polyvinyl chloride) in each case. Given that the coil's outermost loop has a 4 cm diameter, interception of the solution boundary in a manner that places a significant component of the electric field perpendicular to the boundary is ensured. A wide range of NaCl concentrations was tested (0 to 1 M, in 0.1 M increments) so that any limitations to the linearity predicted by the model could be tested in addition to boundary effects — note that the analytical solution was obtained under the restriction that conductivity must be less than ~ 10 S/m. Here we tested solutions ranging from 0 S/m up to ~ 9 S/m, which is above the conductivity expected in any biological medium. Conductivity of each NaCl solution, at 25°C, was determined using a Metler Toledo Seven2Go conductivity meter. Coil loss was obtained by positioning the coil alongside the column in a hands-free manner, to eliminate noise from hand capacitance.

In addition to measured loss, a direct comparison of experiment with theory is obtained by computing the expected coil loss from a discretized version (finite element) of the analytical mapping equation (Section 2). A finite element mesh matching the shape of the included liquid was built for each column of liquid, typically consisting of $\sim 100,000$ elements. The coil has a build-up of 1.0 mm of PCB material over the outermost set of coil loops, and with the 0.5 mm spacing between loop sets, an average distance between coil and liquid column was set equal to wall thickness plus 1.25 mm. The 1.75 cm, 2.3 cm and 3.98 cm internal diameter columns were filled to give a solution height = 16.0 cm, while the coil center was placed at a height of 8.0 cm along the outer wall. The 5.1 cm diameter column was filled to a height of 14.0 cm, while the coil center was placed at a height of 7.0 cm. The 7.7 cm diameter column was filled to a height of 12.0 cm, while the coil center was placed at a height of 6.0 cm.

Figures 1(a) through 1(d) show the results of coil loss measurements for the coil placed flush against the walls of each of the columns. Beginning with the smallest column diameter, where the discrepancy between theory and experiment is greatest, the discrepancy gradually disappears while progressing to the largest columns, where column diameter exceeds coil diameter. In all cases, however, the variation of coil loss with solution electrical conductivity is always linear and through the origin, as predicted by theory. Together with earlier results [9], we conclude that our mapping equation is a viable tool for accomplishing tomographic reconstruction of an electrical conductivity distribution within human tissues.

Our explanation for slope discrepancy is that relative permittivity suddenly drops from ~ 80 for the solution phase down to ~ 3.0 for PVC and then again to 1.0 for air just outside the PVC wall — a violation of an assumption leading to our analytical mapping equation. Because of the disagreement between theory and experiment in cases of very large relative permittivity discontinuities, image reconstruction based upon the mapping formula could lead to a contrast error — i.e., a region would indicate either a larger or smaller conductivity than expected, depending upon whether the "interior region" has higher or lower relative permittivity, though also dependent on the magnitude of the permittivity discontinuity.

Figures 2(a) and 2(b) show the effect of column diameter more directly by considering just a

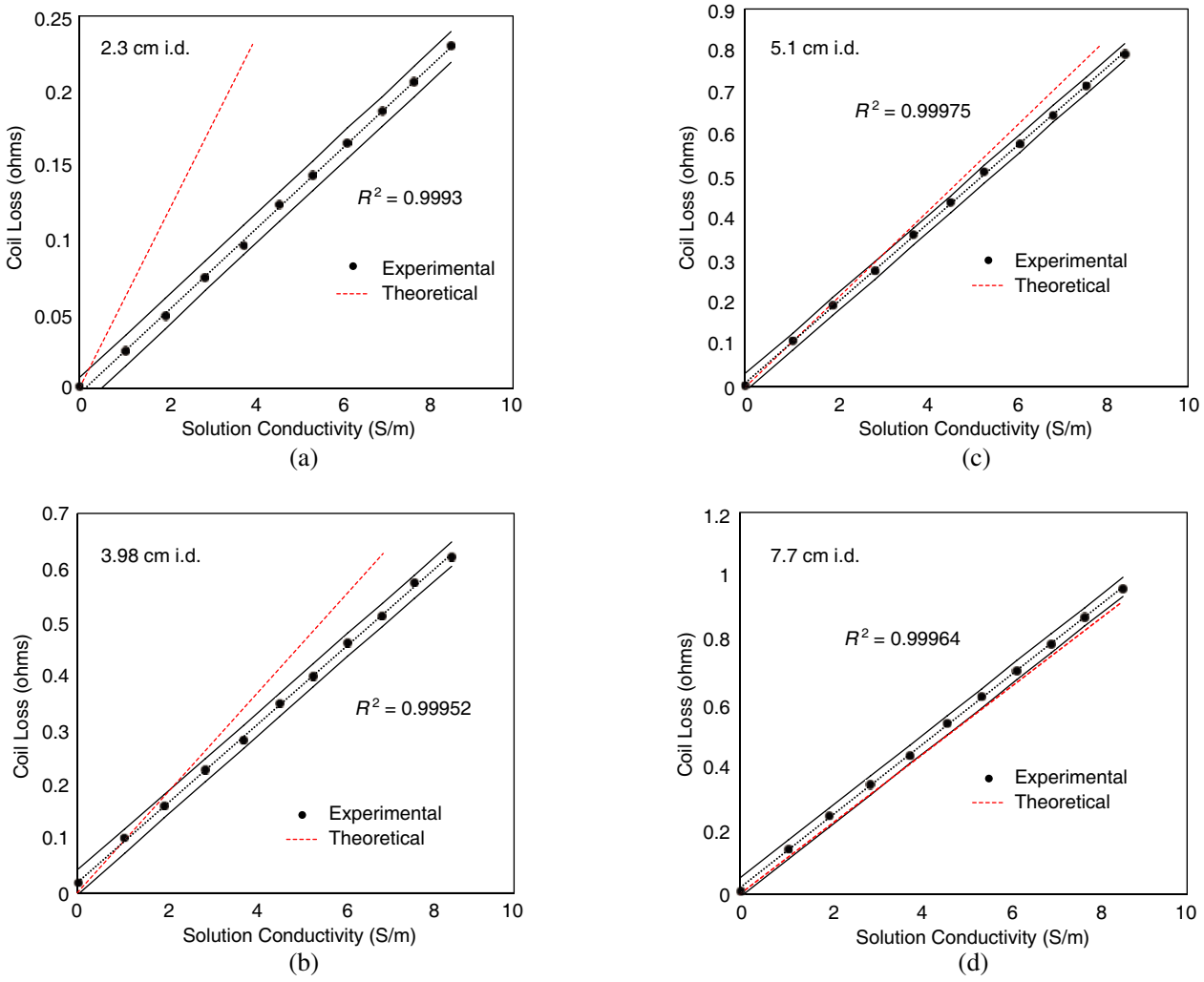

Figure 1. Coil loss for PVC columns filled with salt solutions; coil diameter = 4.0 cm; graphs show 99% confidence intervals; (a) i.d. = 2.3 cm; (b) i.d. = 3.98 cm; (c) i.d. = 5.1 cm; (d) i.d. = 7.7 cm.

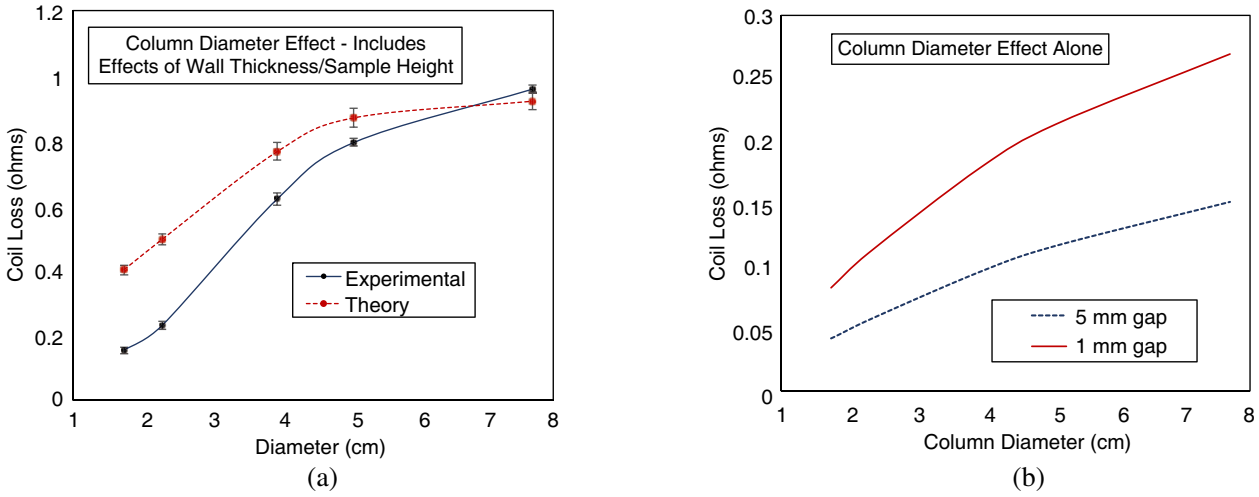

Figure 2. (a) Column diameter impact on measured coil loss; solution conductivity = 8.57 S/m; error bars on theory curve are due to a wall thickness variability of ±0.25 mm; (b) effects of wall thickness and column height removed; column height = 16.0 cm; conductivity = 1.0 S/m.

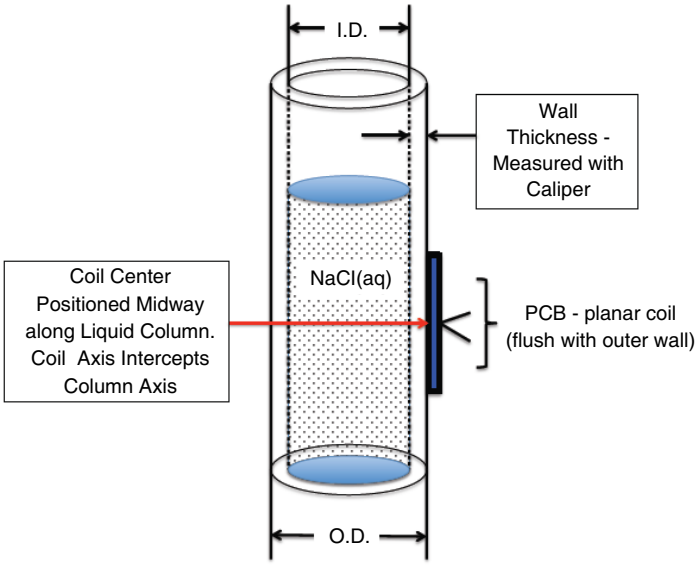

Figure 3. Sketch showing placement of double-layer, PCB-based coil against column wall; note that liquid column height varies with column I.D. (inner diameter) and O.D. (outer diameter) — only the liquid column is meshed.

single conductivity, 8.57 S/m and 1.0 S/m respectively. As column diameter increases in Figure 2(a), the discrepancy between theory and experiment disappears, with data at the highest column diameter showing no significant difference between theory and experiment. Since the experimental procedure involved changing both wall thickness and column height, Figure 2(b) is included to illustrate the effect of column diameter alone, at two different coil-column spacing's. Figure 2(b) illustrates that coil loss is slightly more sensitive to column diameter when coil diameter is less than one column diameter. Future work will investigate the nature of this curve for alternate coil designs.

In reality, the large jumps in relative permittivity explored here are not encountered in practice, even in the case of bone adjacent to muscle — relative permittivities for muscle, bone and fat are $\sim$ 100, 50 and 35, respectively. Even with large, sudden changes in relative permittivity, as shown in [14],

image reconstruction through inversion of Equation (1) is not impaired, though there does appear to be some minor amount of contrast error in cases of extreme relative permittivity change. Consequently, given further progress in instrumentation design, and improvement in image reconstruction algorithms centered around Equation (1), we expect that single-coil MIT will eventually become useful for low-cost, portable imaging applications.

REFERENCES

1. Borcea, L., "Electrical impedance tomography," *Inverse Problems*, Vol. 18, R99–R136, 2002.
2. Sikora, J., *Boundary Element Method for Impedance and Optical Tomography*, Oficyna Wydawnicza Politechniki Warszawskiej, ISBN: 978-83-7207-728-8, 2007.
3. Sikora, J. and S. Wòjtowicz, *Industrial and Biological Tomography: Theoretical Basis and Applications*, Wydawnictwo Książkowe Instytutu Elektrotechniki, ISBN: 978-83-61956-04-4, 2010.
4. Wei, H. Y. and M. Soleimani, "Electromagnetic tomography for medical and industrial applications: Challenges and opportunities," *Proc. IEEE*, Vol. 101, 559–564, 2013.
5. Harpen, M. D., "Influence of skin depth on NMR coil impedance," *Phys. Med. Biol.*, Vol. 33, No. 3, 329–337, 1988.
6. Zaman, A. J. M., S. A. Long, and C. G. Gardner, "The impedance of a single-turn coil near a conducting half space," *J. Nondestructive Eval.*, Vol. 1, No. 3, 183–189, 1980.
7. Harpen, M. D., "Influence of skin depth on NMR coil impedance. Part II," *Phys. Med. Biol.*, Vol. 33, No. 5, 597–605, 1988.
8. Hoult, D. I. and P. C. Lauterbur, "The sensitivity of the zeugmatographic experiment involving human samples," *J. Magnetic Resonance*, Vol. 34, No. 2, 425–433, 1979.
9. Feldkamp, J. R., "Single-coil magnetic induction tomographic three-dimensional imaging," *J. Medical Imaging*, Vol. 2, No. 1, 013502, 2015.
10. Sankowski, D. and J. Sikora, *Electrical Capacitance Tomography: Theoretical Basis and Applications*, Wydawnictwo Książkowe Instytutu Elektrotechniki, ISBN: 978-83-61956-00-6, 2010.
11. Stawicki, K. and S. Gratkowski, "Optimization of signal coils in the magnetic induction tomography system," *Przeglad Elektrotechniczny*, Vol. 86, No. 5, 74–77, 2010.
12. Gradshteyn, I. S. and Ryzhik, *Table of Integrals, Series and Products*, Corrected and Enlarged Edition, A. Jeffrey, Academic Press, New York, NY, 1980.
13. Lapidus, L. and G. F. Pinder, *Numerical Solution of Partial Differential Equations in Science and Engineering*, Wiley-Interscience, J. Wiley & Sons, NY, 1982.
14. Feldkamp, J. R. and S. Quirk, "Effects of tissue heterogeneity on single-coil, scanning MIT imaging," *Proc. SPIE 9783, Medical Imaging: Physics of Medical Imaging*, 978359, 2016.